COMPENSATION OF GEOMETRIC DISTORTION EFFECTS ON INTRAOPERATIVE MAGNETIC RESONANCE IMAGING FOR ENHANCED VISUALIZATION IN IMAGE-GUIDED NEUROSURGERY

Neculai Archip, Ph.D.
Brigham and Women's Hospital, Harvard Medical School, Boston, Massachusetts

Olivier Clatz, Ph.D.
Brigham and Women's Hospital, Harvard Medical School, Boston, Massachusetts

Stephen Whalen, B.Sc.
Brigham and Women's Hospital, Harvard Medical School, Boston, Massachusetts

Simon P. DiMaio, Ph.D.
Brigham and Women's Hospital, Harvard Medical School, Boston, Massachusetts

Peter M. Black, M.D., Ph.D.
Brigham and Women's Hospital, Harvard Medical School, Boston, Massachusetts

Ferenc A. Jolesz, M.D.
Brigham and Women's Hospital, Harvard Medical School, Boston, Massachusetts

Alexandra Golby, M.D.
Brigham and Women's Hospital, Harvard Medical School, Boston, Massachusetts

Simon K. Warfield, Ph.D.
Brigham and Women's Hospital, Harvard Medical School, Boston, Massachusetts

Reprint requests:
Ferenc A. Jolesz, M.D,
Department of Radiology,
Brigham and Women's Hospital,
Harvard Medical School,
75 Francis Street,
Boston, MA 02115.
Email: jolesz@bwh.harvard.edu

Received, August 25, 2006.
Accepted, July 31, 2007.

OBJECTIVE: Preoperative magnetic resonance imaging (MRI), functional MRI, diffusion tensor MRI, magnetic resonance spectroscopy, and positron-emission tomographic scans may be aligned to intraoperative MRI to enhance visualization and navigation during image-guided neurosurgery. However, several effects (both machine- and patient-induced distortions) lead to significant geometric distortion of intraoperative MRI. Therefore, a precise alignment of these image modalities requires correction of the geometric distortion. We propose and evaluate a novel method to compensate for the geometric distortion of intraoperative 0.5-T MRI in image-guided neurosurgery.

METHODS: In this initial pilot study, 11 neurosurgical procedures were prospectively enrolled. The scheme used to correct the geometric distortion is based on a nonrigid registration algorithm introduced by our group. This registration scheme uses image features to establish correspondence between images. It estimates a smooth geometric distortion compensation field by regularizing the displacements estimated at the correspondences. A patient-specific linear elastic material model is used to achieve the regularization. The geometry of intraoperative images (0.5 T) is changed so that the images match the preoperative MRI scans (3 T).

RESULTS: We compared the alignment between preoperative and intraoperative imaging using 1) only rigid registration without correction of the geometric distortion, and 2) rigid registration and compensation for the geometric distortion. We evaluated the success of the geometric distortion correction algorithm by measuring the Hausdorff distance between boundaries in the 3-T and 0.5-T MRIs after rigid registration alone and with the addition of geometric distortion correction of the 0.5-T MRI. Overall, the mean magnitude of the geometric distortion measured on the intraoperative images is 10.3 mm with a minimum of 2.91 mm and a maximum of 21.5 mm. The measured accuracy of the geometric distortion compensation algorithm is 1.93 mm. There is a statistically significant difference between the accuracy of the alignment of preoperative and intraoperative images, both with and without the correction of geometric distortion ($P < 0.001$).

CONCLUSION: The major contributions of this study are 1) identification of geometric distortion of intraoperative images relative to preoperative images, 2) measurement of the geometric distortion, 3) application of nonrigid registration to compensate for geometric distortion during neurosurgery, 4) measurement of residual distortion after geometric distortion correction, and 5) phantom study to quantify geometric distortion.

KEY WORDS: Image-guided neurosurgery, Magnetic resonance image geometric distortion, Multimodal registration, Nonrigid registration

Neurosurgery 62[ONS Suppl 1]:ONS209–ONS216, 2008 DOI: 10.1227/01.NEU.0000297081.51540.45

Interventional magnetic resonance imaging (iMRI) was introduced to enhance intraoperative visualization and has been found to increase the volume of resected low-grade tumors (2, 3, 15, 23). Several recent studies have demonstrated the effectiveness of iMRI

in achieving gross tumor resection (9, 29). Because functional magnetic resonance imaging (fMRI) of tactile, motor, and language tasks is feasible in patients with cerebral tumors (21), several groups have recently proposed integration of functional data into neuronavigation systems (16). Diffusion tensor imaging (DTI) provides information about normal tumor course, displacement or interruption of white matter tracts around the tumor, and fiber-bundle widening that results from edema or tumor. Consequently, efforts have been made in the last years to combine DTI with neurosurgical navigation systems (24, 34). Therefore, the goal of advanced image-guided neurosurgery systems is to accurately align the preoperatively acquired images (fMRI and DTI) with the images obtained intraoperatively during tumor resection (1).

Important geometric distortions often occur in MRI that lead to pixel shifts in the acquired images (21, 35). Several reports describe the importance of these variations, which can be several millimeters in certain areas of the field of view and thus hinder the precise localization of anatomic structures (32).

MRI geometric distortion is caused by artifacts that violate the assumptions of spatial encoding in MRI. These artifacts can be categorized into those characteristic of the imaging hardware and those resulting from patient characteristics. The sources of machine-induced magnetic resonance geometric distortion includes static field inhomogeneity, gradient field nonlinearity, and the presence of eddy currents caused by gradient switching. The distortions induced by gradient nonlinearity and main magnetic field nonuniformity are independent of the patient's position within the scanner. These can be corrected independent of other machine-induced distortions. Sources of patient-induced geometric distortion include magnetic susceptibility effects, chemical shift, and flow.

The vendors of clinical MRI systems often provide software for gradient distortion correction. However, recent studies have estimated the residual gradient distortions (6, 25, 36, 37) and have shown that significant distortions are present even after the gradient distortion correction software is applied. Methods for correcting machine-induced geometric distortion are presented by Doran et al. (11), Langlois et al. (17), and Wang et al. (36, 37). The correction of geometric distortion in stereotactic MRI for neurosurgery (10, 20, 38) and bilateral subthalamic stimulation in Parkinson's disease (19) have also been investigated.

Geometric distortion is also commonly encountered when intraoperative MRI scanners are used. For instance, Petersch et al. (24) report maximum distortions of 28 mm (mean, 2.2 mm) that were measured within the field of view in the frequency-encode direction. However, individuals receiving MRI-guided therapies would also benefit from correction of patient-induced geometric distortion. To the best of our knowledge, there is no proposed method that can compensate for these distortions during clinical interventions.

In this report, we measure the distortion between preoperative and intraoperative images. We also present a novel technique based on a nonrigid registration scheme to reduce the geometric distortion in a 0.5-T open magnet in the context of iMRI-guided neurosurgery. This technique compensates for both machine- and patient-induced distortions. We describe the technical aspects of our method, its implementation, and its validation. We show that this novel method enables accurate alignment of preoperative datasets to intraoperative images and thus provides neurosurgeons with enhanced information during tumor resection.

PATIENTS AND METHODS

Eleven consecutive patients (6 women, 5 men; age range, 28–62 yr; mean, 45.2 yr) with supratentorial gliomas (World Health Organization Grade II, 5 patients; Grade III, 4 patients; Grade IV, 2 patients) were included in our study. All patients underwent surgery at our institution's intraoperative MRI-guided therapy facility between April 2005 and January 2006 for tumors in and adjacent to eloquent brain areas (such as the precentral gyrus and corticospinal tract for motor function and Broca's and Wernicke's areas for language function). For these patients, fMRI and DTI were used for preoperative surgical planning. The study was performed with Institutional Review Board approval and all patients provided informed consent.

Preoperative Imaging

Each patient provided informed consent, and the following preoperative MRI protocol was followed several days before surgery was scheduled to occur. We used a 3-T Signa (General Electric, Milwaukee, WI) scanner.

Anatomic Imaging

We first obtained whole-brain sagittal three-dimensional spoiled, gradient-recalled images in steady state (slice thickness, 1.3 mm; TE/TR, 6/35 ms; flip angle, 75 degrees; field of view [FOV], 24 cm; matrix, 256 $\times$ 256). Subsequently, we obtained axial T2-weighted fast-spin-echo images (slice thickness, 5 mm; TE/TR, 100/3000 ms; FOV, 22 cm; matrix, 512 $\times$ 512).

Functional Magnetic Resonance Imaging

Whole-brain functional images were acquired with a T2*-weighted, echo-planar sequence that was sensitive to the blood oxygen level-dependent signal (TR, 2000 ms; TE, 30 ms; matrix, 64 $\times$ 64 $\times$ 6 mm; FOV, 240 mm; imaging, 24 contiguous slices of 5-mm thickness).

Diffusion Tensor Imaging

Axial line-scan diffusion images (slice thickness, 5 mm; matrix, 512 $\times$ 512; FOV, 24 cm) and echo-planar DTI (matrix, 128 $\times$ 128; phase FOV, 1.0; FOV, 25.6; slice thickness, 3; B value, 800; directions, 31; number of T2, 1) were acquired to cover the entire region of interest as well as "landmark" regions, i.e., areas where the relevant fiber tracts showed high density (e.g., ventral brainstem for the corticospinal tract and lateral geniculate body for the optic radiation).

Magnetic Resonance Spectroscopy

For three patients, we also performed magnetic resonance spectroscopy from the tumor.

Intraoperative Imaging

After the patients were positioned for craniotomy and their heads were fixed using a magnetic resonance-compatible carbon fiber Mayfield clamp (Ohio Medical Instruments, Cincinnati, OH), imaging was performed using the following protocol in the vertically open 0.5-T iMRI unit (SignaSP; General Electric Medical Systems)

with the following parameters. For transverse, sagittal, and coronal T1-weighted, fast spin-echo imaging, the repetition time/echo time (both in milliseconds) was 700/29; FOV, 22 cm; matrix, 256 × 256; number of signals acquired, 1; section thickness, 3 mm; and intersection gap, 1 mm. For transverse, T2-weighted, fast-spin echo imaging, the repetition time/echo time (both in milliseconds) was 5000/99, FOV, 22 cm; matrix, 256 × 256; number of signals acquired, 2; section thickness, 3 mm; and intersection gap, 1 mm. For transverse, three-dimensional, spoiled gradient-echo imaging, the repetition time/echo time (both in milliseconds) was 15.5/5.2; flip angle, 45 degrees; FOV, 22 cm; matrix, 256 × 256; number of signals acquired, 1; section thickness, 2.5 mm; and intersection gap, 0 mm.

Data Processing

Our intraoperative visualization system of multimodal images uses T1-gradient echo (spoiled-gradient echo) sequences to estimate the deformation field that results from brain shift and geometric distortion. We focused our study on the T1-spoiled-gradient echo images. Geometric distortion is present on intraoperative imaging as compared with preoperative 3-T MRI scans (*Fig. 1*). Accurate alignment of preoperative and intraoperative images requires an algorithm to compensate for the geometric distortion. The geometry of intraoperative images is changed to match the preoperative images. We address this by using a nonrigid registration scheme that was first introduced by our group (8) to compensate for brain shift. This registration scheme uses image features to establish correspondence between images. As used here, it estimates a smooth geometric distortion compensation field by regularizing the displacements estimated at the correspondences. A patient-specific linear elastic material model is used to achieve the regularization. The algorithm can be decomposed into three primary parts.

For Part 1, after the preoperative images have been acquired, the patient-specific model is built using image segmentation and mesh generation. Image segmentation is the delineation of structures in the intraoperative data using segmentation strategies that are optimized for the particular type of acquisition. This approach combines the benefits of anatomic information, statistical classification, and elastic matching to achieve results superior to those obtained by any single method alone. Recently, we have also successfully used a method based on a deformable model, which evolves to the brain's surface by the application of a set of locally adaptive model forces (31). For mesh generation, the tetrahedral discretization (volume mesh) of the segmented intracranial cavity provides the basis for a finite-element method of modeling the physical tissue deformation and serves the function of regularizing of the estimated displacements that were obtained from the block-matching step of nonrigid registration. The technique used for tetrahedral mesh generation is described by Fedorov et al. (12). It uses implicit representation of the object as input and produces an adaptive tetrahedral mesh specifically suited for applications that exhibit high deformation. An example of a tetrahedral mesh and its corresponding brain segmentation are presented in *Figure 2*.

From these, a patient-specific model is obtained of the brain material using an incompressible linear elastic constitutive equation.

Part 2 of the algorithm, which is performed intraoperatively, is the block-matching computation for a set of selected blocks on images. This step estimates a set of displacements across the volume.

Part 3 of the algorithm is an iterative hybrid solver that estimates the three-dimensional volumetric deformation field induced by geometric distortion of intraoperative imaging. In this step, the patient-specific model is used to regularize the distortion-compensation field as described in detail by Clatz et al. (8).

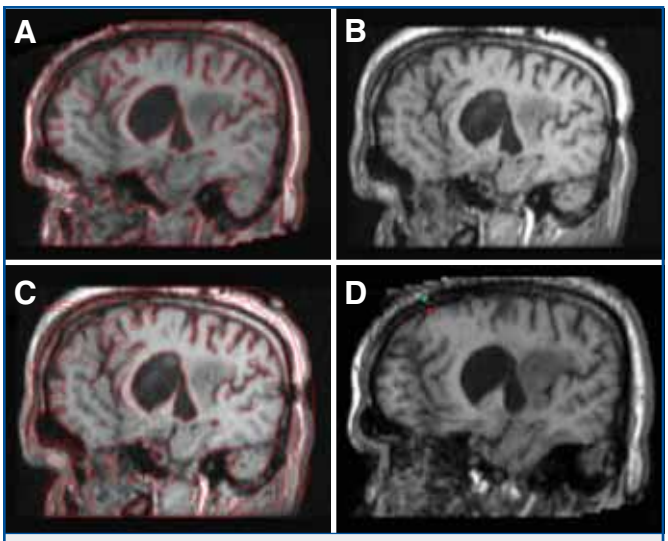

FIGURE 1. *Typical magnetic resonance imaging (MRI) scans from neurosurgery patients who participated in our study.* **A**, *edges of preoperative 3-T MRI scan are extracted with a Canny operator and are drawn in red.* **B**, *intraoperative 0.5-T MRI scan for the same patient, before craniotomy. Significant geometric distortion can be observed.* **C**, *the edges of the 3-T MRI images are displayed over the intraoperative 0.5-T image. The evident misalignment is the result of geometric distortion.* **D**, *landmarks are selected on the preoperative 3-T image* (red) *and on the intraoperative image* (green). *The distance between the two landmarks is the result of geometric distortion.*

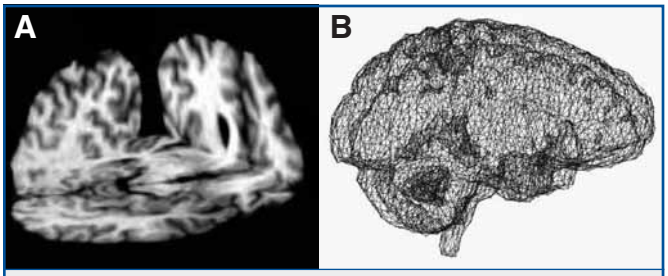

FIGURE 2. **A**, *segmentation of brain from the preoperative MRI scan.* **B**, *mesh generated from the segmentation (***A***) is used to create a biomechanical model of the brain.*

Nonrigid registration algorithms are typically computationally expensive, and parallel computing may be used to accelerate the computation to reduce the computation time to clinically acceptable levels. We have investigated the use of symmetric multiprocessor, cluster, and grid computing hardware to provide accelerated computation (7). Modern hardware enables rapid and effective solution of the system of equations that arises in this approach to geometric distortion.

Geometric Distortion Measurement

The Canny edge detector is commonly used in computer vision to locate sharp intensity changes and find object boundaries in an image (5). The Canny edge detector removes the weak edges using a hysteresis threshold. We used it to extract brain edges from the MRI scans as shown in *Figure 1A*. The edges are distinguished and represented as a set of points.

The Hausdorff metric is a common mathematical measure for comparing two sets of points in terms of their least-similar members. Formally, given two finite point sets:

$A = \{a_1, \ldots, a_p\}$

and

$B = \{b_1, \ldots, b_q\}$

the Hausdorff metric is defined as:

$H(A, B) = \max\{h(A, B), h(B, A)\}$

where:

$h(A, B) = \max_{a \in A} \min_{b \in B} \|a - b\|$ and $\|\cdot\|$ is the Euclidean norm.

The 95% Hausdorff distance is measured between the points on the edges extracted from the two images (the pre- and intraoperative images) with a Canny operator. Ideally, when there are no geometric distortions present, this distance should be zero. Obtaining the 95% Hausdorff value ensures that the outliers are rejected.

RESULTS

Our technique was evaluated while treating 11 consecutive neurosurgery patients. The data were transferred, processed, and displayed in the operating room during the neurosurgical procedure. An example of an intraoperative MRI scan obtained after performing compensation for geometric distortion is presented in *Figure 3*.

In *Figure 4*, alignments among the preoperative DTI and the 3-T T1 MRI scan, the preoperative DTI and the intraoperative 0.5-T T1 MRI scan, and the preoperative DTI and the intraoperative 0.5-T T1 MRI scan after geometric correction are presented. In *Figure 5*, alignments among the preoperative fMRI and 3-T T1 MRI scans, the preoperative fMRI and intraoperative 0.5-T T1 MRI scans, and the preoperative fMRI and intraoperative 0.5-T T1 MRI scans after geometric correction are presented.

The magnitude of the geometric distortion between the images acquired at 0.5 and 3 T is calculated before and after application of the distortion compensation technique using anatomic landmarks and the Hausdorff distance as computed between edges extracted from MRI scans using the Canny operator. Overall, the mean magnitude of the geometric distortion was 10.3 mm, with a minimum of 2.91 mm and a maximum of 21.5 mm. The accuracy for our geometric distortion-compensation algorithm, measured based on the 95% Hausdorff distance, was 1.93 mm.

There was a statistically significant difference between the accuracy of the alignment of pre- and intraoperative images with and without the compensation of geometric distortion ($P < 0.0004$). The complete results are presented in *Table 1*. The registration results have also been reviewed by a team of neurosurgeons from our department and were judged to be adequate.

On a Dell Precision 690n computer (Dell, Round Rock, TX) with four Intel Xeon 5160 processor cores (Intel, Santa Clara, CA) running at 3.0 GHz, execution time is approximately 18 minutes. Additional reductions in computation time are possible if more computers are used.

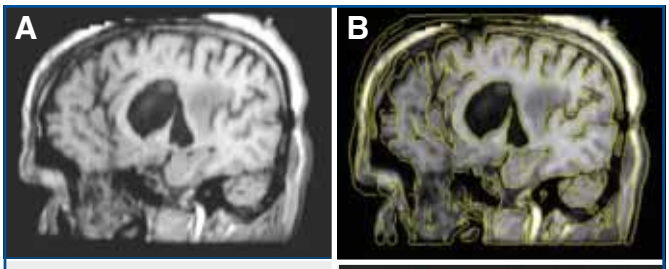

FIGURE 3. *Compensation for geometric distortion.* **A**, *corrected intraoperative 0.5-T image.* **B**, *the same image as in* **A** *reveals the contours extracted from the original intraoperative image. The differences, and the magnitude of the geometric distortion, can be observed.* **C**, *in the corrected intraoperative image, the contours are extracted from the preoperative image. They match well because we have compensated for the distortion.*

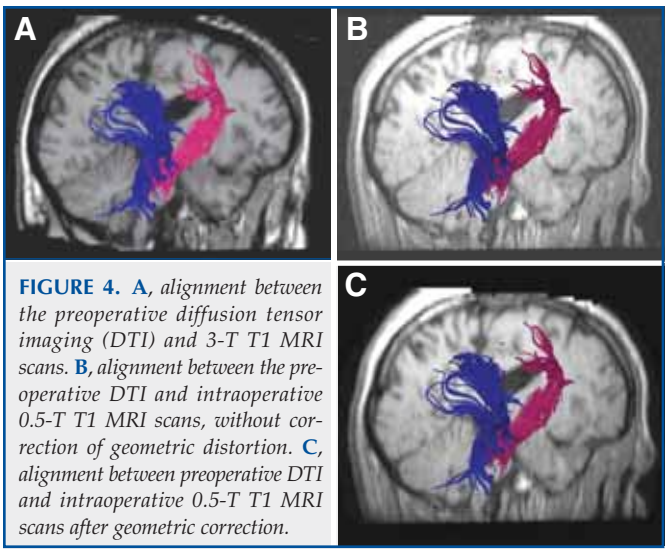

FIGURE 4. **A**, *alignment between the preoperative diffusion tensor imaging (DTI) and 3-T T1 MRI scans.* **B**, *alignment between the preoperative DTI and intraoperative 0.5-T T1 MRI scans, without correction of geometric distortion.* **C**, *alignment between preoperative DTI and intraoperative 0.5-T T1 MRI scans after geometric correction.*

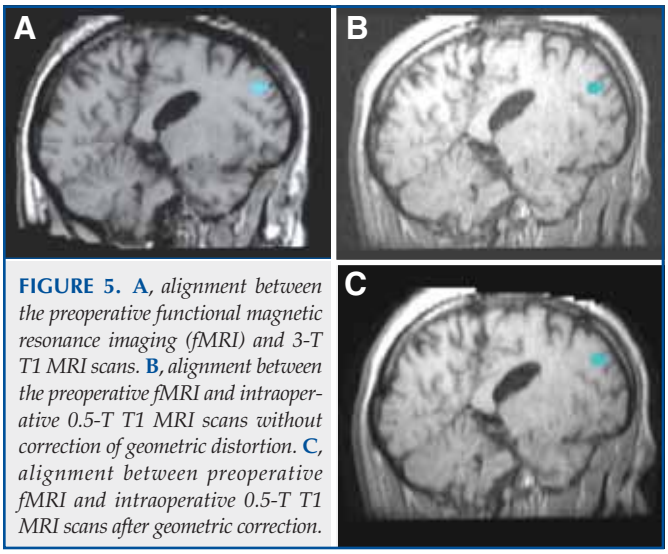

FIGURE 5. **A**, *alignment between the preoperative functional magnetic resonance imaging (fMRI) and 3-T T1 MRI scans.* **B**, *alignment between the preoperative fMRI and intraoperative 0.5-T T1 MRI scans without correction of geometric distortion.* **C**, *alignment between preoperative fMRI and intraoperative 0.5-T T1 MRI scans after geometric correction.*

TABLE 1. Results showing a statistically significant difference between the pre- and postoperative images[a]

Patient no.	Tumor		Geometric distortion magnitude, mm		No correction/ correction ratio
	Position	Pathology (WHO grade)[a]	Before correction	After correction	
1	Right posterior frontal	Oligoastrocytoma (II)	8.10	1.20	6.75
2	Left posterior temporal	Glioblastoma (IV)	15.10	2.40	6.29
3	Left medial temporal	Glioblastoma (IV)	21.50	3.53	6.09
4	Left temporal	Anaplastic oligoastrocytoma (III)	5.70	1.70	3.35
5	Right frontal	Oligoastrocytoma (II)	2.91	0.85	3.42
6	Left frontal	Anaplastic astrocytoma (III)	11.10	2.5	4.44
7	Right medial temporal	Anaplastic astrocytoma (III)	20.00	3.14	6.36
8	Right frontal	Oligoastrocytoma (II)	14.00	2.58	5.42
9	Right frontotemporal	Oligoastrocytoma (II)	5.57	1.20	4.64
10	Right occipital	Anaplastic oligodendroglioma (III)	2.85	0.85	3.35
11	Left frontotemporal	Oligodendroglioma (II)	7.23	1.34	5.39
Average			10.36	1.93	5.04

[a] WHO, World Health Organization.

In addition to assessing the geometric distortion, we have also measured the magnitude of brain deformation that results from tumor resection. The maximum image deformation resulting from both brain shift and geometric distortion was determined to be 21.3 mm. We have previously described in detail our approach to brain-shift quantification (1). Illustrative images of compensation for geometric distortion and brain shift are presented in *Figure 6*.

We also used a General Electric calibration phantom to measure geometric distortion. The phantom was scanned using the same protocol as applied for the neurosurgery patients. Both 3- and 0.5-T images were acquired. Additionally, we scanned the same phantom with a computed tomographic (CT) scan. The disagreement was quantified and represents geometric distortion. The maximum displacement measured with the phantom between the CT scan and the 0.5-T MRI scan was 5 m, and between the CT and the 3-T MRI, it was 1 mm. Results are illustrated in *Figure 7*.

DISCUSSION

Machine-induced MRI distortions have been intensively studied, and several methods to correct them have been proposed. However, patient-induced geometric distortion has received less attention in the context of image-guided neurosurgery.

We identified geometric distortion between preoperative 3-T MRI scans and intraoperative 0.5-T MRI scans. Computed tomography provides images with less geometric distortion. However, the present clinical protocol at our institution does not include any CT imaging for brain neurosurgery at the iMRI. Nevertheless, in our study, we demonstrate that we can improve the accuracy for neurosurgical navigation by compensating for geometric distortion of iMRI. Because our 0.5-T iMRI scanner is only for clinical use, we were unable to scan animals or cadavers.

Instead, we obtained 3- and 0.5-T MRI and CT scans of a General Electric calibration phantom. We measured the differences between these images. Although computed tomography reproduces accurately the geometry of the phantom, we identified differences on 3- and 0.5-T MRI scans. The distortion present on the 0.5-T MRI scan is larger than on the 3-T MRI scan (5 versus 1 mm). Also, based on the anatomic features of the brain MRI scans, qualitative assessment indicates that 3-T images are less distorted than 0.5-T images. Moreover, the 3-T images have higher resolution than the 0.5-T images. Therefore, in our study, we consider the 3-T images as the reference, and modify the geometry of the intraoperative 0.5-T images.

We use the phrase "intraoperative imaging" to describe all imaging performed on the 0.5-T MRI machine, and "preoperative imaging" to describe data acquired to plan the surgery using the 3.0-T MRI machine. These two scanners have different geometric distortion properties, with the 0.5-T MRI scanner having the largest distortion, which must be removed for accurate intraoperative navigation. This distortion can change across the course of the surgery as a result of the craniotomy, but after craniotomy, we also see significant soft-tissue deformation. Our focus here is on compensation for the geometric distortion.

The geometric distortion associated with intraoperative MRI acquisition is a common problem for all existing open-MRI scanners. It is a consequence of both properties of the patient, such as magnetic susceptibility changes resulting from craniotomy, and properties of the magnet design, such as the homogeneity of the static magnetic field. When using an open-magnet design, obtaining a large region of homogeneous, static, magnetic field is a challenging task. For instance, Petersch et al. (24) report maximum distortions of 28 mm (mean, 2.2 mm) within the FOV in the frequency-encode direction. The scanner

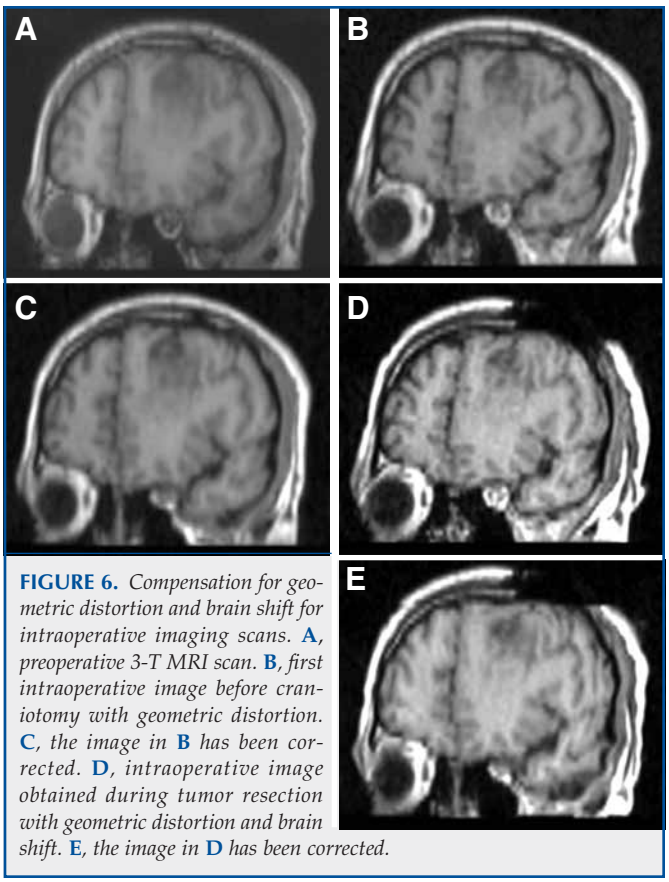

FIGURE 6. *Compensation for geometric distortion and brain shift for intraoperative imaging scans.* **A**, *preoperative 3-T MRI scan.* **B**, *first intraoperative image before craniotomy with geometric distortion.* **C**, *the image in* **B** *has been corrected.* **D**, *intraoperative image obtained during tumor resection with geometric distortion and brain shift.* **E**, *the image in* **D** *has been corrected.*

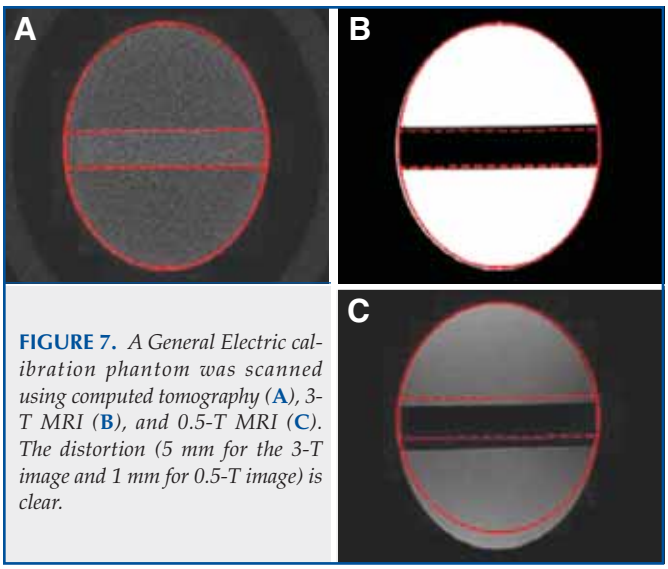

FIGURE 7. *A General Electric calibration phantom was scanned using computed tomography (***A***), 3-T MRI (***B***), and 0.5-T MRI (***C***). The distortion (5 mm for the 3-T image and 1 mm for 0.5-T image) is clear.*

used was a Siemens Magnetom Open Viva 0.2-T resistive MRI scanner (New York, NY). The clinical application was radiotherapy treatment of prostate cancer.

There are many sources of geometric distortion in magnetic resonance imaging, all of which contribute by fundamentally disrupting the assumption of linear encoding of position in space using frequency and phase encoding in MRI scans. Here, we are concerned with identifying, measuring, and compensating for this geometric distortion.

Geometric distortion is present as a result of properties of the scanner; it is subject to and impacts all of the data acquired, even before craniotomy is performed. Soft-tissue deformation such as brain shift occurs only after craniotomy and exists in addition to geometric distortion.

Our group has already presented results regarding image registration for brain-shift compensation, for instance, in studies by Nabavi et al. (22) or more recently, by Ruiz-Alzola et al. (27), Clatz et al. (8), and Archip et al. (1). In the present study, we only focus on the distortion in the images before soft-tissue deformation occurs.

In our study, we measured distortions as large as 21.3 mm. Therefore, for accurate navigation in neurosurgery and even for data fusion restricted to rigid-body transformation, compensation for this geometric distortion is essential.

In this report, we propose a solution to address these distortions using a nonrigid registration scheme. A robust, accurate, and sufficiently rapid nonrigid registration algorithm was used to compensate for geometric distortion. For each patient, we were able to successfully correct the geometric distortion. A clinically compatible execution time was achieved by using parallel computing and by performing key image-processing steps before the surgery.

CONCLUSION

The major contributions of this study are identification of geometric distortion of intraoperative 0.5-T images as compared with preoperative 3-T images, measurement of the size of the geometric distortion, application of nonrigid registration to compensate for geometric distortion during neurosurgery, measurement of the residual distortion after geometric distortion correction, and phantom study to quantify geometric distortion.

As clearly demonstrated, after we applied our correction method, the residual geometric distortion apparent in the corrected images was negligibly small for all patients studied. The introduced technology combined with an advanced neurosurgery navigation system enables the use of high-accuracy navigation with preoperative DTI and fMRI scans during tumor resection.

REFERENCES

1. Archip N, Fedorov A, Lloyd B, Chrisochoides N, Golby A, Black PMcL, Warfield SK: Integration of patient specific modeling and advanced image processing techniques for image guided neurosurgery. Presented at the SPIE Medical Imaging, San Diego, CA, February 17–22, 2006.
2. Black PMcL, Alexander E 3rd, Martin C, Moriarty T, Nabavi A, Wong TZ, Schwartz RB, Jolesz F: Craniotomy for tumor treatment in an intraoperative magnetic resonance imaging unit. **Neurosurgery** 45:423–431, 1999.
3. Black PMcL, Moriarty T, Alexander E 3rd, Stieg P, Woodard EJ, Gleason PL, Martin CH, Kikinis R, Schwartz RB, Jolesz FA: Development and implementation of intraoperative magnetic resonance imaging and its neurosurgical applications. **Neurosurgery** 41:831–842, 1997.

4. Bradley WG: Achieving gross total resection of brain tumors: Intraoperative MR imaging can make a big difference. **AJNR Am J Neuroradiol** 23:248–349, 2002.
5. Canny JF: A computational approach to edge detection. **IEEE Trans Pattern Analysis and Machine Intelligence** 8:679–698, 1986.
6. Chen Z, Ma CM, Paskalev K, Li J, Yang J, Richardson T, Palacio L, Xu X, Chen L: Investigation of MR image distortion for radiotherapy treatment planning of prostate cancer. **Phys Med Biol**. 21:1393–1403, 2006.
7. Chrisochoides N, Fedorov A, Kot A, Archip N, Black PMcL, Clatz O, Golby A, Kikinis R, Warfield SK: Toward real-time image guided neurosurgery using distributed and grid computing. Presented at the Supercomputing, Tampa, FL, November 11–17, 2006.
8. Clatz O, Delingette H, Talos IG, Golby AJ, Kikinis R, Jolesz FA, Ayache N, Warfield SK: Robust non-rigid registration to capture brain shift from intraoperative MRI. **IEEE Trans Med Imaging** 24:1417–1427, 2005.
9. Claus EB, Horlacher A, Hsu L, Schwartz RB, Dello-Iacono D, Talos F, Jolesz FA, Black PMcL: Survival rates in patients with low-grade glioma after intraoperative magnetic resonance image guidance. **Cancer** 103:1227–1233, 2005.
10. Dean D, Kamath J, Duerk JL, Ganz E: Validation of object-induced MR distortion correction for frameless stereotactic neurosurgery. **IEEE Trans Med Imaging** 17:810–816, 1998.
11. Doran SJ, Charles-Edwards L, Reinsberg SA, Leach MO: A complete distortion correction for MR images: I. Gradient warp correction. **Phys Med Biol** 50:1342–1361, 2005.
12. Fedorov A, Chrisochoides N, Kikinis R, Warfield SK: An evaluation of three approaches to tetrahedral mesh generation for deformable registration of MR images. Presented at the IEEE International Symposium on Biomedical Imaging: From Nano to Macro, Arlington, VA, April 6–9, 2006.
13. Haberg A, Kvistad KA, Unsgard G, Haraldseth O: Preoperative blood oxygen level-dependent functional magnetic resonance imaging in patients with primary brain tumors: Clinical application and outcome. **Neurosurgery** 54:902–914, 2004.
14. Hughes DG, Robertson S, Allen PS: Intensity artifacts in MRI caused by gradient switching in an animal-size NMR magnet. **Magn Reson Med** 25:167–179, 1992.
15. Jolesz FA, Nabavi A, Kikinis R: Integration of interventional MRI with computer-assisted surgery. **J Magn Reson Imaging** 13:69–77, 2001.
16. Krishnan R, Raabe A, Hattingen E, Szelenyi A, Yahya H, Hermann E, Zimmermann M, Seifert V: Functional magnetic resonance imaging integrated neuronavigation: Correlation between lesion-to-motor cortex distance and outcome. **Neurosurgery** 55:904–914, 2004.
17. Langlois S, Desvignes M, Constans JM, Revenu M: MRI geometric distortion: A simple approach to correcting the effects of non-linear gradient fields. **J Magn Reson Imaging** 9:821–831, 1999.
18. Maurer CR Jr, Aboutanos GB, Dawant BM, Gadamsetty S, Margolin RA, Maciunas RJ, Fitzpatrick JM: Effect of geometrical distortion correction in MR on image registration accuracy. **J Comput Assist Tomogr** 20:666–679, 1996.
19. Menuel C, Garnero L, Bardinet E, Poupon F, Phalippou D, Dormont D: Characterization and correction of distortions in stereotactic magnetic resonance imaging for bilateral subthalamic stimulation in Parkinson disease. **J Neurosurg** 103:256–266, 2005.
20. Michiels J, Bosmans H, Pelgrims P, Vandermeulen D, Gybels J, Marchal G, Suetens P: On the problem of geometric distortion in magnetic resonance images for stereotactic neurosurgery. **Magn Reson Imaging** 12:749–765, 1994.
21. Mueller WM, Yetkin FZ, Hammeke TA, Morris GL, Swanson SJ, Reichert K, Cox R, Haughton VM: Functional magnetic resonance imaging mapping of the motor cortex in patients with cerebral tumors. **Neurosurgery** 39:515–520, 1996
22. Nabavi A, Black PMcL, Gering DT, Westin CF, Mehta V, Pergolizzi RS Jr, Ferrant M, Warfield SK, Hata N, Schwartz RB, Wells WM 3rd, Kikinis R, Jolesz FA: Serial intraoperative magnetic resonance imaging of brain shift. **Neurosurgery** 48:787–797, 2001.
23. Nimsky C, Ganslandt O, Hastreiter P, Wang R, Benner R, Sorensen AG, Fahlbusch R: Intraoperative diffusion-tensor MR imaging: Shifting of white matter tracts during neurosurgical procedure: Initial experience. **Radiology** 234:218–225, 2005.
24. Petersch B, Bogner J, Fransson A, Lorang T, Potter R: Effects of geometric distortion in 0.2T MRI on radiotherapy treatment planning of prostate cancer. **Radiother Oncol** 71:55–64, 2004.
25. Piepmeier JM, Christopher S, Spencer D, Byrne T, Kim J, Knisel JP, Lacy J, Tsukerman L, Makuch R: Variations in the natural history and survival of patients with supratentorial low-grade astrocytomas. **Cancer** 38:872–878, 1996.
26. Posse S: Direct imaging of magnetic field gradients by group spin-echo selection. **Magn Reson Med** 25:12–29, 1992.
27. Ruiz-Alzola J, Westin CF, Warfield SK, Alberola C, Maier SE, Kikinis R: Nonrigid registration of 3D tensor medical data. **Medical Image Analysis** 6:143–161, 2002.
28. Schenck JF: The role of magnetic susceptibility in magnetic resonance imaging: MRI magnetic compatibility of the first and second kinds. **Med Phys** 23:815–850, 1996.
29. Schneider JP, Trantakis C, Rubach M, Schulz T, Dietrich J, Winkler D, Renner C, Schober R, Geiger K, Brosteanu O, Zimmer C, Kahn T: Intraoperative MRI to guide the resection of primary supratentorial glioblastoma multiforme—A quantitative radiological analysis. **Neuroradiology** 47:489–500, 2005.
30. Skare S, Andersson JL: Correction of MR image distortions induced by metallic objects using a 3D cubic B-spline basis set: Application to stereotactic surgical planning. **Magn Reson Med** 54:169–181, 2005.
31. Smith SM: Fast robust automated brain extraction. **Hum Brain Mapp** 17:143–155, 2002.
32. Sumanaweera TS, Glover G, Song S, Adler J, Napel S: Quantifying MRI geometric distortion in tissue. **Magn Reson Med** 31:40–47, 1994.
33. Sun L, Aletras AH, Schmalbrock P, Skinner TE, Chakeres D, Irsik R, Robitaille PM: Water and fat MR imaging with chemical shift selective 3D steady state methods. **Magn Reson Med** 31:359–364, 1994.
34. Talos IF, O'Donnell L, Westin CF, Warfield SK, Wells WM, Yoo SS, Panych L, Golby A, Mamata H, Maier SE, Ratiu P, Guttmann CG, Black PMcL, Jolesz FA, Kikinis R: Diffusion tensor and functional MRI fusion with anatomical MRI for image guided neurosurgery. Presented at the Sixth International Conference on Medical Image Computing and Computer-Assisted Intervention, Montreal, Canada, November 16–18, 2003.
35. Walton L, Hampshire A, Forster DMC, Kemeny AA: A phantom study to assess the accuracy of stereotactic localization, using T1 weighted magnetic resonance imaging with the Leksell stereotactic system. **Neurosurgery** 38:170–178, 1996.
36. Wang D, Strugnell W, Cowin G, Doddrell DM, Slaughter R: Geometric distortion in clinical MRI systems Part I: Evaluation using a 3D phantom. **Magn Reson Imaging** 22:1211–1221, 2004.
37. Wang D, Strugnell W, Cowin G, Doddrell DM, Slaughter R: Geometric distortion in clinical MRI systems Part II: Correction using a 3D phantom. **Magn Reson Imaging** 22:1223–1232, 2004.
38. Weis J, Ericsson A, Silander HC, Hemmingsson A: Magnetic resonance spectroscopic imaging for visualization and correction of distortions in MRI: High precision applications in neurosurgery. **Magn Reson Imaging** 16:1265–1272, 1998.
39. Wirtz CR, Knauth M, Staubert A, Bonsanto MM, Sartor K, Kunze S, Tronnier VM: Clinical evaluation and follow up results for intraoperative magnetic resonance imaging in neurosurgery. **Neurosurgery** 46:1120–1122, 2000.
40. Zhu XX, Macdonald PM: Empirical compensation function for eddy current effects in pulsed field gradient nuclear magnetic resonance experiments. **Solid State Magn Reson** 4:217–227, 1995.

Acknowledgments

We thank GE for the research support. This investigation was supported in part by National Science Foundation Information Technology Research 0426558; National Multiple Sclerosis Society Award #RG 3478A2/2, a research grant from CIMIT; and by National Institutes of Health grants R03 EB-006515, U41 RR-019703, P01 CA-067165, R01 RR-021885, R03 CA-126466, P30 HD-018655, and R01 HL-074942.

COMMENTS

Multimodality navigation is becoming increasingly popular. Data and images are registered with each other, resulting in a multimodality three-dimensional framework that is used to visualize anatomy, function, metabolism, and other information in the surgical field. This

kind of advanced navigation, even combined with intraoperative imaging, is prone to errors owing to the registration process itself and to varying spatial distortion of the original data from each modality.

Archip et al. present a sophisticated approach to deal with this problem by application of a nonrigid registration algorithm to compensate for the geometric distortion. Their challenge was to register various preoperative 3-T data with their intraoperative 0.5-T data. The 0.5-T data seemed to be most distortion vulnerable, which might be a problem of mid- and low-field magnetic resonance scanners in general. The study focuses on the comparison with 0.5-T intraoperative data, which were acquired before craniotomy. These distortions have to be separated from the effects of intraoperative imaging per se caused by intraoperative events such as brain shift and effects due to the air-brain interface during actual intraoperative imaging.

The solution presented allows integration of multimodality data that were acquired with different magnetic resonance scanners in the intraoperative setting with reliable accuracy by compensating for the distortion effects of the 0.5-T magnetic resonance scanner.

An alternative approach to circumvent this problem is to acquire all different data with the same scanner, preferably in the same setting, so that the patient's individual effects remain the same. In our setup of intraoperative high-field magnetic resonance imaging (MRI) applying a 1.5-T scanner, functional MRI (fMRI), diffusion tensor imaging (DTI), and magnetic resonance spectroscopy are all performed with the same machine. Imaging after head fixation before surgery is repeated intraoperatively after resection of a tumor to evaluate the extent of resection and to visualize shifted major white matter tracts with intraoperative fiber tracking. A side-by-side display of the identical pre- and intraoperative images, which were measured at the identical slice positions, greatly facilitates image interpretation and reduces the intraoperative time needed for advanced registration algorithms. Nevertheless, nonlinear registration of preoperative data with intraoperative images is an important tool. When preoperative data cannot be obtained easily during surgery, the approach presented allows registering them reliably with intraoperative images.

Christopher Nimsky
Erlangen, Germany

Archip et al. describe a novel system for geometric distortion correction as applied to surgery for brain tumor resection using preoperative imaging (including MRI, fMRI, DTI, magnetic resonance spectroscopy, and positron emission tomography) fused to intraoperative MRI studies. The authors describe a case series of 11 patients undergoing resection of tumors in or near eloquent brain regions. The authors found a 10.3-mm mean magnitude and 21.5-mm maximum magnitude of geometric distortion measured on intraoperative images. By using their compensation algorithm, this was reduced to an average of 1.93 mm.

This work is important as it highlights a potential source of bias in combining preoperative studies to interventional imaging and offers a novel solution to this problem. Whether this technology will increase safety, improve outcomes, or prove to be a reasonable surrogate for awake surgery must be determined with further studies.

Andres M. Lozano
Toronto, Canada

This is an excellent article by the group that basically invented intraoperative MRI (iMRI). They have used a clever, nonrigid registration technique to morph the geometrically distorted 0.5-T iMRI T1-weighted spoiled gradient echo (SPGR) technique to a less-distorted SPGR image at 3-T. Using a phantom, they show that 3-T SPGR differs from computed tomography (the "gold standard") by 1 mm, whereas 0.5-T iMRI differs by 5 mm. The reason for doing this is to be able to fuse 3-T preoperative DTI and fMRI to the intraoperative 0.5-T images.

I have a relatively minor problem with this article. The DTI and fMRI images are both based on echo planar imaging techniques, which are much more susceptible to geometric distortion than SPGR, particularly at 3-T. This is particularly a problem near the cranial base where diamagnetic susceptibility effects (brain versus air) distort echo-planar–based images. Thus, whereas the SPGR anatomic images may be accurately morphed, neurosurgeons using iMRI should be aware that DTI and fMRI images may not be.

William G. Bradley, Jr.
San Diego, California